A novel three-dimensional notch fracture criterion via effective critical distances

Mirmilad Mirsayar*, Behnam Shahbazian

Department of Aerospace, Physics, and Space Sciences, Florida Institute of Technology, Melbourne, Florida 32901, USA

Abstract

Many well-known fracture criteria rely on a mode-independent parameter measured under pure mode *I* loading conditions, called the critical distance, which is traditionally considered a material property representing the size of the fracture processing zone. Recent studies have unveiled the potential for significantly increased accuracy in fracture criteria by utilizing a mode-dependent critical distance in calculations. In response to this revelation, the concept of effective critical distance (ECD) was recently introduced and successfully examined in cracked components under in-plane and out-of-plane loading conditions, both theoretically and experimentally. In this work, for the first time, the concept of ECD is introduced for V- and U-shaped notches to form a new three-dimensional notch fracture criterion based on the maximum principal strain (MPSN). The fracture angle and the onset of fracture predicted by the proposed criterion are theoretically compared to other existing criteria, and experimentally, to the test data presented in the literature. It is shown that the developed criterion can more accurately predict the mixed-mode $I/II/III$ fracture behavior of V- and U-notched components which accentuates the profound significance of embracing the ECD concept in constructing three-dimensional fracture criteria.

Keywords: Notched components; brittle fracture; fracture toughness; mixed-mode I/II/III; effective critical distance; strain-based framework

effective critical distance; V- and U-notch; three-dimensional brittle fracture; mixed-mode fracture toughness; strain-based framework

1. Introduction

Unlike cracks which are a sign of damage in the structures, notches are an important part of structural design because they are used for various purposes such as joining two parts, transferring load from one part to another, etc. Since stress concentration is high at the tip of a notch, it is expected that the crack starts propagating at this location and subsequently, causes fracture in the structure [1, 2]. In most applications, notches are usually subjected to mixed mode $I/II/III$ loading conditions which is a combination of three basic modes of deformation known as mode I (opening), mode II (in-plane shear), and mode III (out-of-plane shear) loadings [3]. To prevent catastrophic incidents from happening, foreseeing the fracture behavior in structures is of utmost importance and has been the subject of many studies in the past decades. For instance, based on the ductility of the material which can affect the plastic zone size at the tip of the stress raisers [4-12], several fracture criteria have been proposed by researchers to predict when and how crack nucleation and ultimately fracture happens. Brittle mixed-mode $I/II/III$ fracture criteria are mathematical expressions that typically measure an energy/strain/stress parameter at a certain distance from the crack tip, called critical distance ($\mathrm{r_c}$), and the fracture is anticipated when the measured parameter at $r = r_c$ reaches its critical value [13-39]. Several studies have been conducted over the years to increase the accuracy of the fracture criteria and/or make them applicable to both in-plane and out-of-plane loading conditions [3, 40]. In what follows, some of them are addressed briefly.

Two famous stress-based fracture criteria are maximum tangential stress (MTS) [41] and maximum principal stress (MPS) for in-plane and out-of-plane fracture modes, respectively [42,

43]. Point-stress (PS) criterion [44] is another stress-based fracture criterion which is an extension of the MTS criterion for investigating mixed-mode brittle fracture in cracked components. Since stress-based fracture criteria are relatively simpler than the other two criteria categories (i.e., energy- and strain-based), one approach to increase the accuracy is to add the effect of higher-order terms (e.g., the T-stress) to the fracture model [35-40].

Energy-based criteria were initially limited to in-plane loading modes and among the early proposed criteria, one can refer to the energy release rate (ERR) [13] and the strain energy density (SED) [14] criteria. According to the mentioned criteria, crack propagation is expected in the direction where ERR reaches its maximum value and SED becomes minimum, respectively. Later, they have been extended to be used for analyzing out-of-plane fracture modes in cracked and notched components as well [15-20].

Even though strain-based criteria have never been as popular as the other two fracture criteria among the researchers, the well-known maximum tangential strain criterion (MTSN) [23], suitable for in-plane loading modes, falls into this category which its more precise version later was developed by adding the effects of the first nonsingular tangential strain term (i.e., T–strain) to it [22]. The precision of the extended criterion, named EMTSN, has been validated by conducting numerous tests with various brittle and quasi-brittle materials and geometries. Ultimately, it was shown that the EMTSN criterion is noticeably more accurate than many traditional criteria in predicting the onset of fracture and the fracture angle [24-29]. The competence of strain-based criteria in evaluating fracture behavior in specimens subjected to in-plane and out-of-plane loading conditions is not fully understood yet. Nonetheless, the development of appropriate fixtures for performing accurate three-dimensional fracture tests has drawn researchers' attention to pursuing their research using different approaches [45- 48].

Due to the simpler forms of in-plane fracture models, the number of criteria developed under these conditions is far higher than the out-of-plane ones; some of the latter can be found here [17,18,49-52]. This shows that complexity has always been a nuisance to researchers, and they have always tried to somehow circumvent it in developing their fracture theories and at the same time achieve more accuracy in their predictions. For example, as noted before, adding higher-order terms to the solution is one approach but not only it increases the computational cost, but also may cause losing the physical meaning of the problem hence, even a reasonable number of added higher-order terms are a matter of dispute among the researchers. The situation becomes even more dramatic when it comes to dealing with more complex material systems such as orthotropic or bi-materials [36, 53-55]. Other recent efforts in this field include development of computational approaches to understand mixed-mode fracture behavior in notched (and cracked components) under mixed-mode loading conditions. Examples are those developed using Peridynamics [56 – 60], phase-field [61 – 63], and finite element [64, 65] methods. While numerous works exist on computational modeling of fracture under three-dimensional loading conditions, a considerable portion lacks computational efficiency and is limited to in-plane loading conditions. In addition, alongside these computational approaches, theoretical analysis in this field retains a top-tier significance to advance the field by developing fundamental principles, concepts, and frameworks, thereby fostering a deeper understanding of underlying mechanisms and relationships in three-dimensional fracture mechanics of notched components.

As mentioned earlier, the concept of critical distance plays an important role in developing various fracture criteria. Interestingly, even though the length of the critical distance significantly varies with the mode mixity, conventionally, it has been considered a mode-independent parameter measured only under pure mode I loading conditions and reckoned as a material property.

Traditionally, the size of the critical distance can be formulated as $r_c = \frac{\alpha}{\pi}\left(\frac{K_{Ic}}{\sigma_t}\right)^2$ where σ_t is the tensile strength of the material, K_{Ic} is the mode I fracture toughness, and the coefficient α can obtain any value from 0.5 to 2 depending on the chosen approach (e.g., line methods, point methods, etc.) [66-68].

Recent studies have shown [55, 69, 70] that by considering a mode-dependent critical distance (i.e., the effective critical distance (ECD)) in the fracture criterion, more precision can be achieved while maintaining physical crack tip characteristics. So far, the ECD has been combined with the maximum principal strain (MPSN) and the maximum tangential strain energy density (MTSED) criteria to construct two novel fracture criteria, namely, ECD-SN and ECD-MTSED [55, 69]. In both cases, which are for cracks only, the ECD proved to be tremendously effective in increasing the accuracy and relatively maintaining the simplicity of the solution [55, 69, 70]. However, the ECD concept has not yet been applied to notched components, a gap which will be addressed in the current investigation.

In this study, for the first time, the concept of the ECD is applied to the notched components (V- and U-shaped notches) to construct a novel three-dimensional fracture criterion capable of predicting fracture behavior under mixed-mode $I/II/III$ loading conditions. Then, the results obtained from this approach are compared to those acquired from existing notch fracture criteria including mean stress criterion (MS), PS, and MTS [71- 74] criteria as well as the experimental data reported in the literature. Finally, the accuracy of each approach in predicting the experimental results is studied and discussed. The following sections consist of the theoretical framework (Section 2), which includes some general remarks about elastic stress fields around a notch tip followed by the development of the theory, and, results and discussion (Section 3), where the

developed theoretical framework will be examined by the experimental data. Finally, the conclusion of this research is described in Section 4.

2. Theoretical framework

This section is dedicated to the theoretical part of the current study. First, the equations of the elastic stress fields near the tip of U- and V-notches are expressed in Section 2.1. These equations are used later in Section 2.2. to obtain the maximum principal strain around the notch tip under mixed-mode I/II/III conditions. Finally, a three-dimensional strain-based fracture criterion is developed in Section 2.2 for notched components using the concept of effective critical distances.

2.1. Elastic stress fields for U- and V-notches

The solution for the elastic stress fields in the neighborhood of sharp V- shaped notches was first proposed by Williams [75]. Later, a solution for U- and round-tip V-shaped notches under in-plane and out-of-plane loading conditions was developed by Filippi et al. [76] and Zappalorto et al. [77], respectively. According to [76, 77], the linear-elastic stress fields around a blunt V-notch under mixed-mode $I/II/III$ loading can be written as

$$\begin{Bmatrix}\sigma_{\theta\theta}\\ \sigma_{rr}\\ \tau_{r\theta}\end{Bmatrix}=\frac{K_I r^{\lambda_1-1}}{\sqrt{2\pi}}\left[\begin{Bmatrix}X_{\theta\theta}(\theta)\\ X_{rr}(\theta)\\ X_{r\theta}(\theta)\end{Bmatrix}^{(I)}+\left(\frac{r}{r_0}\right)^{\mu_1-\lambda_1}\begin{Bmatrix}Y_{\theta\theta}(\theta)\\ Y_{rr}(\theta)\\ Y_{r\theta}(\theta)\end{Bmatrix}^{(I)}\right]+\frac{K_{II} r^{\lambda_2-1}}{\sqrt{2\pi}}\left[\begin{Bmatrix}X_{\theta\theta}(\theta)\\ X_{rr}(\theta)\\ X_{r\theta}(\theta)\end{Bmatrix}^{(II)}+\left(\frac{r}{r_0}\right)^{\mu_2-\lambda_2}\begin{Bmatrix}Y_{\theta\theta}(\theta)\\ Y_{rr}(\theta)\\ Y_{r\theta}(\theta)\end{Bmatrix}^{(II)}\right], \quad (1)$$

$$\tau_{rz}=\frac{K_{III} r^{\lambda_3-1}}{\sqrt{2\pi}}\left[\sin(\lambda_3\theta)+\left(\frac{r}{r_3}\right)^{\mu_3-\lambda_3}\sin(\mu_3\theta)\right], \quad (2)$$

$$\tau_{\theta z}=\frac{K_{III} r^{\lambda_3-1}}{\sqrt{2\pi}}\left[\cos(\lambda_3\theta)+\left(\frac{r}{r_3}\right)^{\mu_3-\lambda_3}\cos(\mu_3\theta)\right], \quad (3)$$

$$\sigma_{zz}=\begin{cases}0 & \text{plane stress}\\ \nu(\sigma_{rr}+\sigma_{\theta\theta}) & \text{plane strain}\end{cases}, \quad (4)$$

where K_I, K_{II}, and K_{III} are modes I, II, and III notch stress intensity factors (NSIFs), respectively (note that the dimension of K is not always $\text{MPa}.\sqrt{\text{m}}$). The angular functions $X_{ij}(\theta)$ and $Y_{ij}(\theta)$

are given in Appendix A and μ_i $(i \equiv 1,2,3)$ are reported in [76] as functions of α (half of the notch opening angle, see Fig. 1). Needless to say, when notch opening angle is zero, the blunt V-notch becomes a U-notch. The eigenvalues λ_i $(i \equiv 1,2)$ can be obtained by solving two characteristic equations:

$$\sin(\lambda_1 q\pi) + \lambda_1 \sin(q\pi) = 0, \text{ for mode } I, \tag{5a}$$

$$\sin(\lambda_2 q\pi) - \lambda_2 \sin(q\pi) = 0, \text{ for mode } II, \tag{5b}$$

and λ_3 can be found as:

$$\lambda_3 = \frac{\pi}{2(\pi-\alpha)} = \frac{1}{q}. \tag{6}$$

The parameter r_0 can be obtained as shown in Fig. 1 depending on notch tip radius ρ, and r_3 can be estimated as $r_3 \cong (1-\mu_3)\,\rho$ [77].

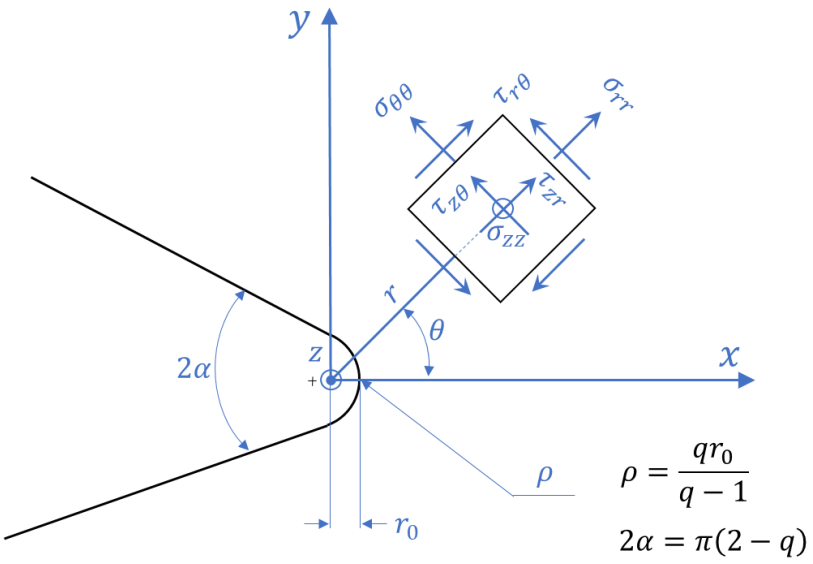

Fig. 1. Schematic of a round-tip V-notch with associated polar coordinates and stresses.

2.2. Development of ECD-SN criterion for notches: N-ECD-SN criterion

The traditional version of the maximum principal strain criterion (MPSN) postulates that crack start propagating when the maximum principal strain (ε_p) reaches to its critical value (ε_c) at a fixed (i.e., mode independent) critical distance of r_c from the crack front. This criterion has been modified recently in [55] by introducing a mode-dependent critical distance (effective critical distance: ECD) for cracks exposed to mixed-mode $I/II/III$ displacement modes. Following the same approach for notches, we have

$$\frac{\partial \varepsilon_p}{\partial \theta}\Big|_{r=r_c,\ \theta=\theta_0} = 0\ , \frac{\partial^2 \varepsilon_p}{\partial \theta^2}\Big|_{r=r_c,\ \theta=\theta_0} < 0, \tag{7}$$

$$\varepsilon_p\big|_{r=r_c,\ \theta=\theta_0} = \varepsilon_c\ , \tag{8}$$

where θ_0 is the in-plane ($r-\ \theta$) kinking angle. Having known that the principal strains occur in $\theta - z$ plane [55], ε_p can be expressed by

$$\varepsilon_p = \frac{\varepsilon_{\theta\theta}+\varepsilon_{zz}}{2} + \frac{1}{2}\sqrt{(\varepsilon_{\theta\theta}-\varepsilon_{zz})^2 + 4\varepsilon_{\theta z}^2}\ , \tag{9}$$

considering the plane strain conditions ($\varepsilon_{zz} = 0$, $\sigma_{zz} = \nu(\sigma_{rr} + \sigma_{\theta\theta})$), we have

$$\varepsilon_p = \frac{\varepsilon_{\theta\theta}}{2} + \frac{1}{2}\sqrt{\varepsilon_{\theta\theta}^2 + 4\varepsilon_{\theta z}^2}\ , \tag{10}$$

where

$$\varepsilon_{\theta\theta} = \frac{1+\nu}{E}[(1-\nu)\sigma_{\theta\theta} - \nu\sigma_{rr}], \tag{11}$$

$$\varepsilon_{\theta z} = \frac{1+\nu}{E}\tau_{\theta z}\ . \tag{12}$$

Assuming that the critical strain is independent of notch geometry (i.e., ε_c is a material property), we can express ε_c as [55]:

$$\varepsilon_c = (1+\nu)(1-2\nu)\frac{\sigma_t}{E}\,, \tag{13}$$

where E and ν represent the Young's modulus and the Poisson's ratio of the material, respectively. Substituting Eqs. (1) and (3) into Eqs. (11) and (12), and setting $p_i = 1-\lambda_i$ and $m_i = \mu_i - \lambda_i$, yields:

$$\varepsilon_{\theta\theta} = \frac{1-\nu^2}{E\sqrt{2\pi}}\left[\frac{K_I}{r^{p_1}}\left(X^I_{\theta\theta}(\theta) + \frac{\mathrm{r}^{m_1}}{\mathrm{r_0}^{m_1}}Y^I_{\theta\theta}(\theta)\right) + \frac{K_{II}}{r^{p_2}}\left(X^{II}_{\theta\theta}(\theta) + \frac{\mathrm{r}^{m_2}}{\mathrm{r_0}^{m_2}}Y^{II}_{\theta\theta}(\theta)\right)\right] - \frac{\upsilon(1+\nu)}{E\sqrt{2\pi}}\left[\frac{K_I}{r^{p_1}}\left(X^I_{rr}(\theta) + \frac{\mathrm{r}^{m_1}}{\mathrm{r_0}^{m_1}}Y^I_{rr}(\theta)\right) + \frac{K_{II}}{r^{p_2}}\left(X^{II}_{rr}(\theta) + \frac{\mathrm{r}^{m_2}}{\mathrm{r_0}^{m_2}}Y^{II}_{rr}(\theta)\right)\right], \tag{14}$$

$$\varepsilon_{\theta z} = \frac{K_{III}(1+\nu)}{E\sqrt{2\pi}}\left[r^{-p_3}\cos(\lambda_3\theta) + \frac{r^{m_3-p_3}}{r_0^{m_3}}\cos(\mu_3\theta)\right]. \tag{15}$$

Considering an effective critical distance of $r_{c,e}$ (instead of the traditional constant r_c that is measured under pure mode *I* loading conditions) the onset of fracture should satisfy the following conditions:

$$\varepsilon_p\left(r_{c,e},\theta_0\right) = \frac{\varepsilon_{\theta\theta}}{2} + \frac{1}{2}\sqrt{\varepsilon^2_{\theta\theta} + 4\varepsilon^2_{\theta z}}\Big|_{\substack{r=r_{c,e}\\ \theta=\theta_0}} = \frac{(1+\nu)(1-2\nu)}{E}\sigma_t\,. \tag{16}$$

For a given notch configuration (i.e., ρ, α), the effective critical distance, $r_{c,e}$, can be expressed by a general function as:

$$r_{c,e} = \prod(K_I, K_{II}, K_{III}, K_{Ic}, K_{IIc}, K_{IIIc}, \sigma_t, \nu, \theta_0)\,. \tag{17}$$

While an explicit closed-form solution may not be attainable to describe the function Π, the expression for pure modes, shown in Fig. 2, can be obtained as follows:

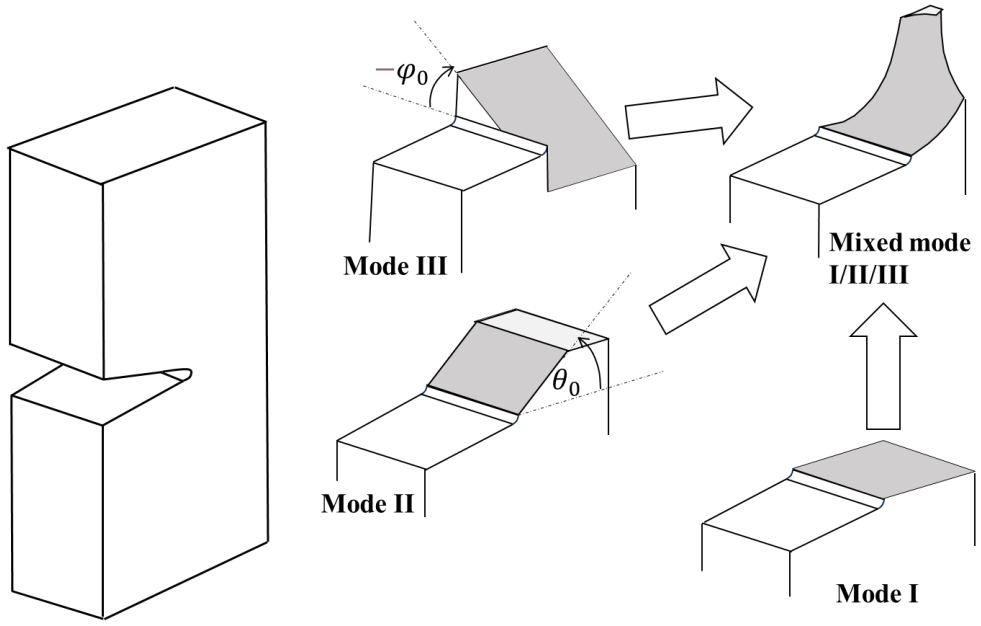

Fig. 2. Schematic of different modes of fracture near the tip of a blunt V-notch.

A. Considering pure mode I conditions (i.e., $K_{II} = K_{III} = \theta_0 = 0, r_{c,e} = r_{c,I}$):

$$\varepsilon_p\left(r_{c,e}, \theta_0 = 0\right) = \varepsilon_{\theta\theta}\left(r_{c,I}, \theta_0 = 0\right) = \frac{K_{Ic}}{E\sqrt{2\pi}}\left[\frac{\left(1-\nu^2\right)}{r^{p_1}}\left(X^I_{\theta\theta}(0) + \frac{\mathrm{r}^{m_1}}{\mathrm{r_0}^{m_1}} Y^I_{\theta\theta}(0)\right) - \frac{\upsilon(1+\nu)}{r^{p_1}}\left(X^I_{rr}(0) + \frac{\mathrm{r}^{m_1}}{\mathrm{r_0}^{m_1}} Y^I_{rr}(0)\right)\right]\Big|_{r=r_{c,I}}, \tag{18}$$

The Eq. (18) can be rewritten as:

$$\varepsilon_p\left(r_{c,I}, 0\right) = \frac{K_{Ic}}{E}\left(A_I r_{c,I}^{-p_1} + B_I r_{c,I}^{m_1-p_1}\right) = \varepsilon_c\,, \tag{19}$$

where,

$$A_I = \frac{\left(1-\nu^2\right)X^I_{\theta\theta}(0) - \nu(1+\nu)X^I_{rr}(0)}{\sqrt{2\pi}}\,, \tag{20}$$

$$B_I = \frac{\left(1-\nu^2\right)Y^I_{\theta\theta}(0) - \nu(1+\nu)Y^I_{rr}(0)}{r_0^{m_1}\sqrt{2\pi}}\,. \tag{21}$$

It is interesting to mention that for the special case of a U-notch (i.e., $\alpha = 0$), we get $\lambda_1 = 0.5$, $\mu_1 = -0.5$, and thus $p_1 = 0.5$ and $m_1 = -1$. Therefore, the Eq. (19) can be expressed in a simple form of:

$$A_I r_{c,I}^{-0.5} + B_I r_{c,I}^{-1.5} = (1+\nu)(1-2\nu)\frac{\sigma_t}{K_{Ic}} . \tag{22}$$

B. Considering pure mode II conditions (i.e., $K_I = K_{III} = 0, \theta_0 = \theta_{II} \neq 0, r_{c,e} = r_{c,II}$):

$$\varepsilon_p\left(r_{c,II}, \theta_0\right) = \varepsilon_{\theta\theta}\left(r_{c,II}, \theta_0\right) = \frac{K_{IIc}}{E}\left(A_{II}(\theta_{II}) r_{c,II}^{-p_2} + B_{II}(\theta_{II}) r_{c,II}^{m_2 - p_2}\right) = \varepsilon_c , \tag{23}$$

where, $A_{II}(\theta_{II})$ and $B_{II}(\theta_{II})$ can be expressed as:

$$A_{II}(\theta_{II}) = \frac{(1-\nu^2) X_{\theta\theta}^{II}(\theta_{II}) - \nu(1+\nu) X_{rr}^{II}(\theta_{II})}{\sqrt{2\pi}} , \tag{24}$$

$$B_{II}(\theta_{II}) = \frac{(1-\nu^2) Y_{\theta\theta}^{II}(\theta_{II}) - \nu(1+\nu) Y_{rr}^{II}(\theta_{II})}{r_0^{m_2}\sqrt{2\pi}} . \tag{25}$$

However, in Eq. (23), both θ_{II} and $r_{c,II}$ are unknown. To find both unknown parameters, an additional equation is required. The second equation can be formed by satisfying Eq. (7), as:

$$\left.\frac{\partial \varepsilon_p}{\partial \theta}\right|_{\substack{r=r_{c,II} \\ \theta=\theta_{II}}} = r_{c,II}^{-p_2}\frac{\partial A_{II}(\theta)}{\partial \theta} + r_{c,II}^{m_2 - p_2}\left.\frac{\partial B_{II}(\theta)}{\partial \theta}\right|_{\theta=\theta_{II}} = 0 . \tag{26}$$

Now, by solving Eqs. (23) and (26) simultaneously using the proper approach (e.g., Newton-Raphson method) both θ_{II} and $r_{c,II}$ can be found.

Equations (23) and (26) can be rewritten for U-notches by putting $\lambda_2 = 0.5$ and $\mu_2 = -0.5$. That is:

$$\begin{cases} A_{II}(\theta_{II}) r_{c,II}^{-0.5} + B_{II} r_{c,II}^{-1.5} = (1+\nu)(1-2\nu)\frac{\sigma_t}{K_{Ic}} , \\ r_{c,II}^{-0.5}\frac{\partial A_{II}(\theta_{II})}{\partial \theta_{II}} + r_{c,II}^{-1.5}\frac{\partial B_{II}(\theta_{II})}{\partial \theta_{II}} = 0 \end{cases} \Longrightarrow \theta_{II}, r_{c,II} \tag{27}$$

C. For pure mode III conditions (i.e., $K_I = K_{II} = \theta_0 = 0, r_{c,e} = r_{c,III}$)

$$\varepsilon_p\left(r_{c,III}, 0\right) = \varepsilon_{\theta z} = \frac{(1+\nu)}{E}\frac{K_{IIIc} r_{c,III}^{-p_3}}{\sqrt{2\pi}}\left[1 + \left(\frac{r_{c,III}}{r_3}\right)^{m_3}\right] = \varepsilon_c \ , \tag{28}$$

substituting Eq. (13) into Eq. (28), gives

$$r_{c,III}^{-p_3} + \frac{r_{c,III}^{m_3 - p_3}}{r_3^{m_3}} = \frac{(1-2\nu)\sqrt{2\pi}}{K_{IIIc}}\sigma_t \ . \tag{29}$$

For a U-notch, $\lambda_3 = 0.5$, $\mu_3 = 0.41$, $p_3 = 0.5$, and $m_3 = -0.09$, thus we have:

$$r_{c,III}^{-0.5} + r_3^{0.09}\left(r_{c,III}^{-0.59}\right) = \frac{(1-2\nu)\sqrt{2\pi}}{K_{IIIc}}\sigma_t \ . \tag{30}$$

The twisting angle φ_0 (i.e., out-of-plane fracture angle) under mixed-mode conditions (any θ_0) can be obtained by [50]:

$$\varphi_0 = \frac{1}{2}\tan^{-1}\left[\frac{2\varepsilon_{\theta z}}{\varepsilon_{\theta\theta}}\right]\Big|_{\theta=\theta_0} = \frac{1}{2}\tan^{-1}\left[\frac{2\tau_{\theta z}}{(1-\nu)\sigma_{\theta\theta} - \nu\sigma_{rr}}\right]\Big|_{\theta=\theta_0} . \tag{31}$$

Ultimately, according to [55, 69], the effective critical distance $r_{c,e}$ under mixed-mode $I/II/III$ loading conditions can be defined by (see Appendix A in [69] for details)

$$r_{c,e} = \sqrt{\left(\beta_I r_{c,I}\right)^2 + \left(\beta_{II} r_{c,II}\right)^2 + \left(\beta_{III} r_{c,III}\right)^2} \ , \tag{32}$$

where

$$\beta_j = \frac{\sqrt{\omega_j}}{\sqrt{\omega_I + \omega_{II} + \omega_{III}}} \ , \ \omega_j = \frac{K_j}{K_{jc}} \ , j \equiv I, II, III \ \ . \tag{33}$$

By substituting the solutions of $r_{c,i}$ ($i \equiv I, II, III$) for notches from Eqs. (19), (23), (26), and (28) into Eq. (32), $r_{c,e}$ can be obtained under the given mixed-mode $I/II/III$ conditions. Thus, the onset

of mixed mode $I/II/III$ fracture can be computed by Eq. (16) using $r_{c,e}$ calculated in Eq. (30), where the required in-plane fracture angle θ_0 is found by

$$\frac{\partial}{\partial\theta}\left[\varepsilon_{\theta\theta}+\sqrt{\varepsilon_{\theta\theta}^2+4\varepsilon_{\theta z}^2}\right]\Big|_{\substack{r=r_{c,e}\\ \theta=\theta_0}}=0 \;\longrightarrow \theta_0 \quad . \tag{34}$$

Substituting the computed kinking angle θ_0 from Eq. (34) into Eq. (31) provides us with the corresponding out-of-plane fracture angle φ_0.

3. Results and discussion

In this section, the fracture toughness and the fracture angle of U- and V- notches obtained from the proposed criterion are theoretically compared to the data acquired from various well-known fracture criteria (e.g., MTS, MS, PS, etc.), and experimentally, to test and predict the data reported in the literature.

To this end, normalized mode II (i.e., p_c) and mode III (i.e., q_c) fracture toughness parameters are defined in Eq. (35). Also, a traditional processing zone size for U- and V-notches (i.e., $r_{c,v}$) is presented in Eq. (35a).

$$r_{c,v}=r_0+\frac{1}{2\pi}\left(\frac{K_{Ic}}{\sigma_t}\right)^2, \tag{35a}$$

$$p_c=\left(\frac{K_{IIc}}{K_{Ic}}\right)r_{c,v}^{\lambda_2-\lambda_1}, \tag{35b}$$

$$q_c=\left(\frac{K_{IIIc}}{K_{Ic}}\right)r_{c,v}^{\lambda_3-\lambda_1}. \tag{35c}$$

Moreover, to plot fracture angle curves, the mode mixity parameters $M_{I/II}^e$, $M_{I/III}^e$, and $M_{III/II}^e$, respectively for mixed-mode I/II, I/III, and III/II, are defined in Eq. (36):

$$M_{I/II}^e=\frac{2}{\pi}tan^{-1}\left[\left(\frac{K_I}{K_{II}}\right)r_{c,v}^{\lambda_1-\lambda_2}\right], \tag{36a}$$

$$M_{I/III}^e=\frac{2}{\pi}tan^{-1}\left[\left(\frac{K_I}{K_{III}}\right)r_{c,v}^{\lambda_1-\lambda_3}\right], \tag{36b}$$

$$M^{e}_{III/II} = \frac{2}{\pi} tan^{-1}[(\frac{K_{III}}{K_{II}}) r_{c,v}^{\lambda_3 - \lambda_2}]. \quad (36c)$$

The plots of mixed-mode fracture toughness as well as in-plane and out-of-plane fracture angles can be created theoretically in terms of normalized fracture toughness values and mode mixity parameters (very similar to Appendix B in [22] for cracks). Due to the lack of experimental data for the mixed-mode II/III fracture toughness and in-plane (θ_0) and out-of-plane fracture angle (φ_0) in the literature, herein, the authors have decided to solely present the theoretical results obtained from the proposed method in Figs. 3 and 4. In Fig. 3a, the mixed-mode II/III fracture toughness is plotted where the V-notch opening angle (2α) and the notch tip radius (ρ) are equal to 120° and 0.5 mm, respectively. Also, the Poisson's ratio (ν) and the relative fracture toughness values (p_c, q_c) are chosen arbitrarily. Fig. 3b depicts the variation of mixed-mode II/III fracture toughness for the same notch tip radius but different notch opening angles. Since under the mixed-mode II/III loading conditions both in-plane and out-of-plane fracture angles occur, they are plotted in Fig.4a and b, respectively. In this figure, the V-notch opening angle and the notch tip radius are constant, but the Poisson's ratio varies. As can be seen in Fig. 4, by raising Poisson's ratio, the out-of-plane fracture angle increases but the in-plane fracture angle decreases.

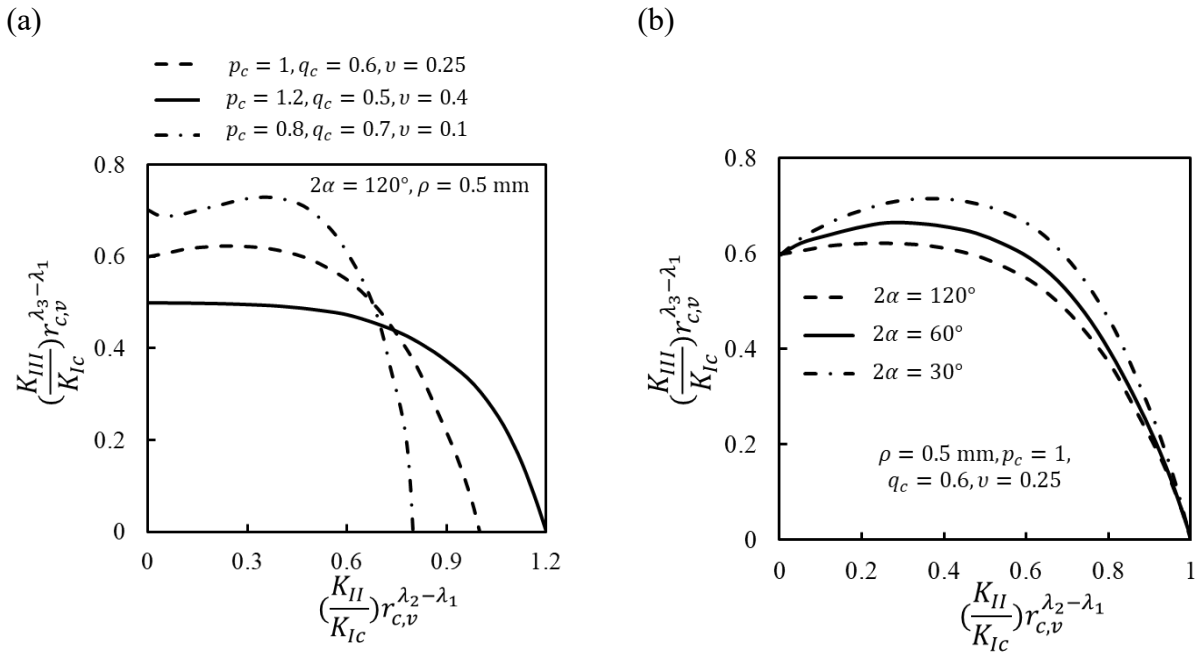

Fig. 3. Mixed-mode II/III fracture toughness variations computed by the N-ECD-SN criterion proposed in the current work: a) for $2\alpha = 120°$, $\rho = 0.5mm$ and arbitrary values of p_c, q_c, and υ, b) for $\rho = 0.5\ mm, p_c = 1, q_c = 0.6,\ \upsilon = 0.25$ and different values of the notch opening angle 2α.

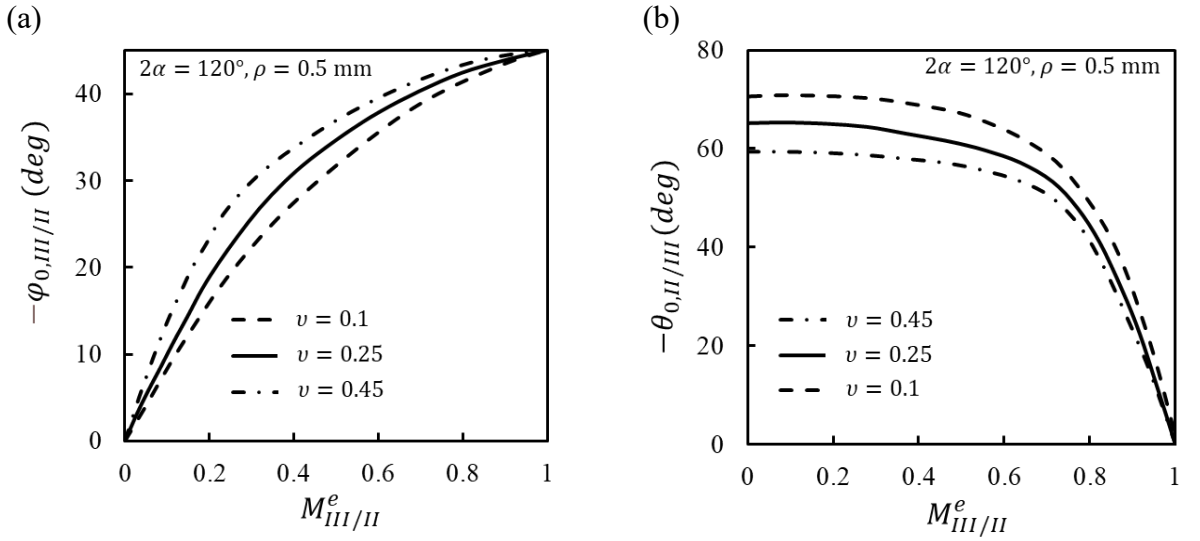

Fig. 4. Theoretical effects of mode mixity and the Poisson's ratio on the fracture angles under mixed-mode II/III conditions computed by the N-ECD-SN criterion (for $2\alpha = 120°$, $\rho = 0.5mm$): a) out-of-plane fracture angle, b) in-plane fracture angle.

Fig. 5 compares the test data for the mixed-mode I/III fracture toughness of round bars made of graphite and weakened by a V-notch to the theoretical results obtained from the PS and the

proposed criterion (N-ECD-SN) for two different notch opening angles. As illustrated in this figure, the N-ECD-SN criterion by far outperforms the PS criterion.

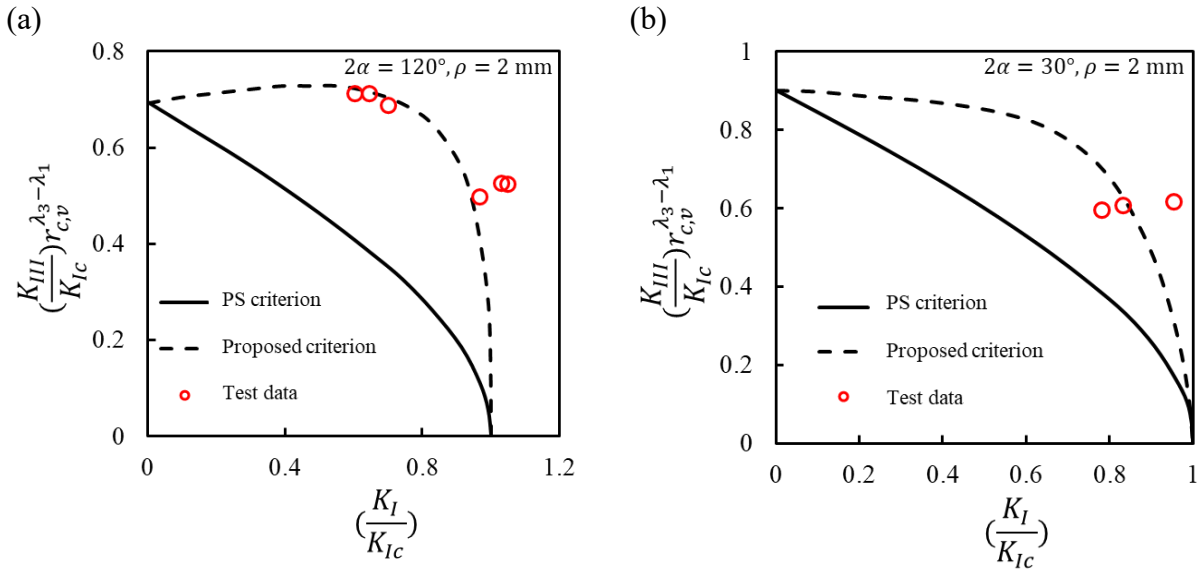

Fig. 5. Mixed-mode I/III fracture test data for V-notched graphite round bars [3, 78] (notch tip radius of $\rho = 2mm$ and different notch opening angles 2α) together with the theoretical predictions of PS and N-ECD-SN criteria: a) $2\alpha = 120°$, and b) $2\alpha = 30°$.

The theoretical data on mixed-mode I/II fracture toughness and kinking angle for U-notched graphite specimens are compared to the experimental data for two different notch tip radii in Fig. 6. According to this figure, for both notch tip radii, the prediction curves of MTS and MS criteria are almost identical to each other, and they underestimate the actual fracture toughness and overestimate the experimental kinking angle. However, the curve obtained from the proposed criterion is skewed towards the test data and passes among them like a trend line and clearly shows higher accuracy.

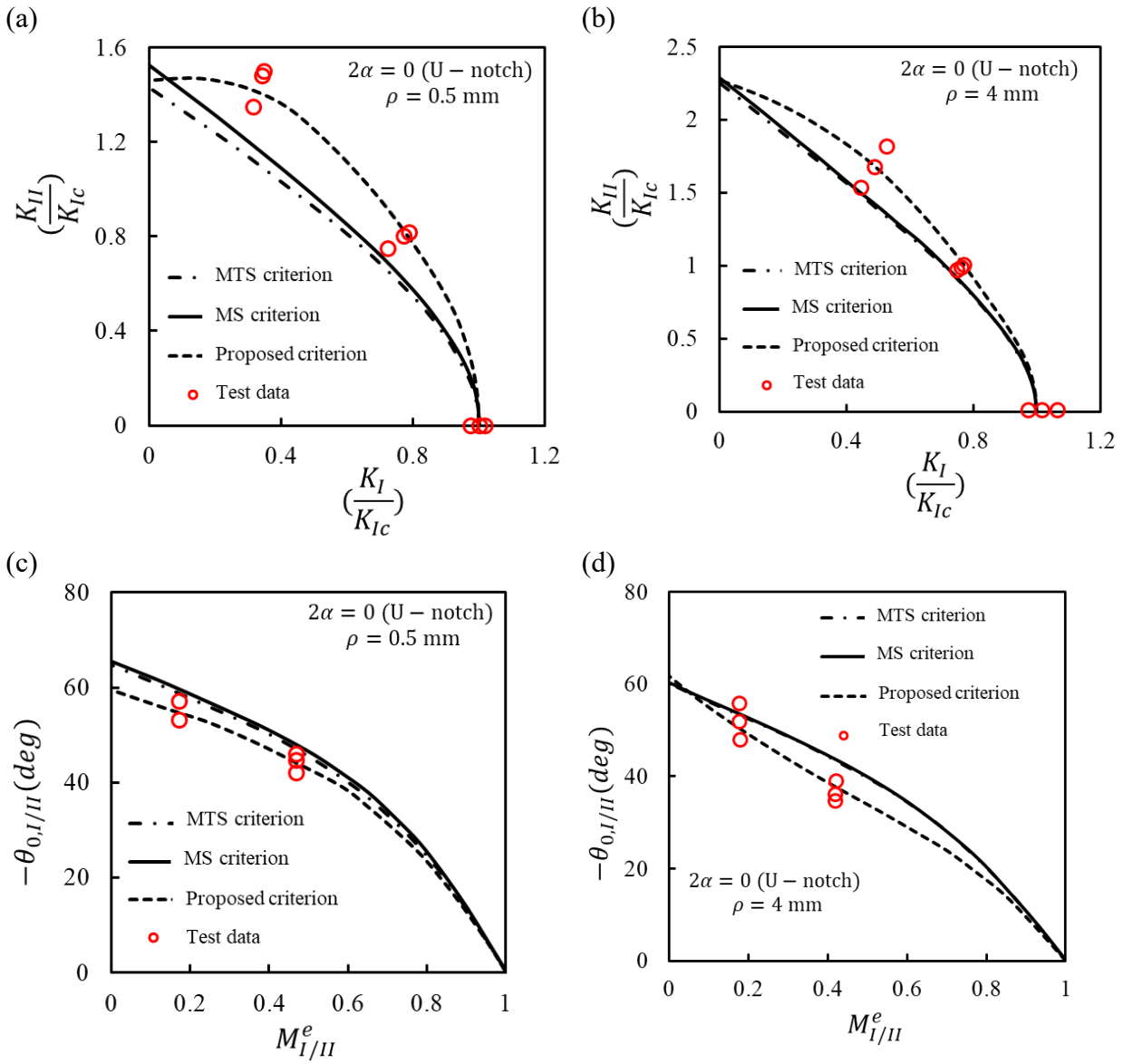

Fig. 6. Theoretical mixed-mode I/II fracture curves by the MTS, MS, and N-ECD-SN criteria together with the experimental results for U-notched graphite specimens: mixed-mode I/II fracture toughness for a) $\rho = 0.5mm$, b) $\rho = 4mm$; in-plane I/II fracture angle versus different mode mixities for c) $\rho = 0.5mm$, and d) $\rho = 4mm$ [79].

Out-of-plane I/III Fracture toughness and fracture angle of U-notched PMMA specimens for two different notch tip radii are illustrated in Figs. 7a, b and Figs. 7c, d, respectively. Regarding the fracture curves (Figs. 7a, b), it can be seen that the N-ECD-SN criterion evidently gives better prediction than the PS and MS criteria. Concerning the fracture angle and according to Fig. 7c and

d, all criteria give a good prediction but the curve from the proposed criterion seems more promising.

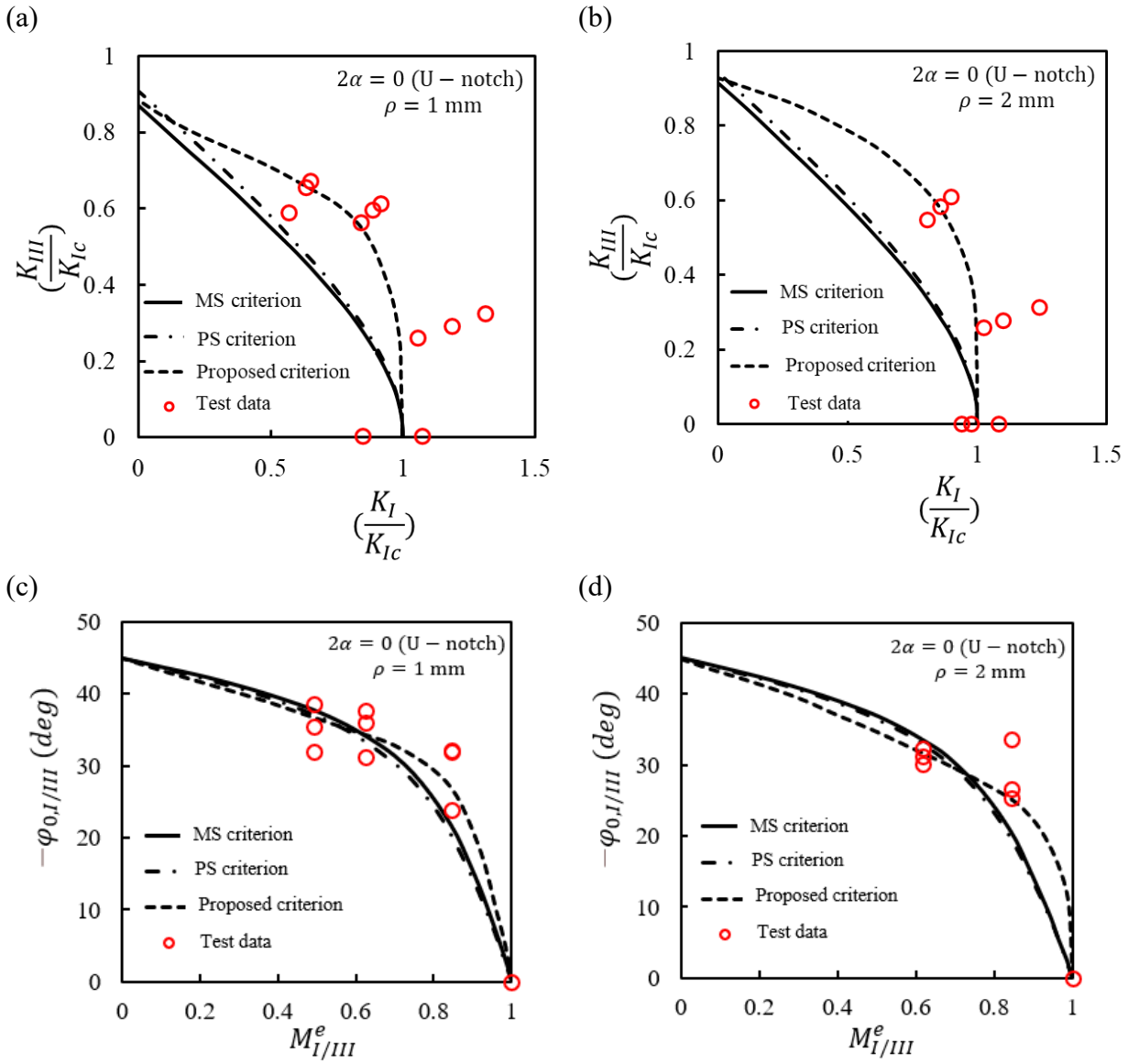

Fig. 7. Theoretical mixed-mode I/III fracture curves by the MS, PS, and N-ECD-SN criteria together with the experimental results for U-notched PMMA specimens: mixed-mode I/III fracture toughness for a) $\rho = 1mm$, b) $\rho = 2mm$; out-of-plane I/III fracture angle versus different mode mixities for c) $\rho = 1mm$, and d) $\rho = 2mm$ [80].

Fig. 8, shows the out-of-plane mixed-mode I/III fracture behavior of V-notched specimens made of Polystyrene for two different notch tip radii. According to [81, 82] for brittle and quasi-brittle materials subjected to mode III dominant loading conditions, a more accurate theoretical prediction can be obtained by using a modified critical distance of $d_{c,v} = r_0 + d_c$ where like before r_0 is the space from the origin of the coordinate system behind the notch tip to the notch tip itself and d_c is the critical distance measured from the notch tip, calculated by

$$d_c = \frac{2}{\pi}\left(\frac{K_{III_c}}{\sigma_t}\right)^2. \tag{37}$$

As shown in Fig. 8a, the MS criterion underestimates but the N-ECD-SN criterion gives a good average of the test data. The same interpretation of fracture toughness can be applied to Fig. 8b denoting higher precision of the ECD-based criterion. Figs. 8 c, d show the twisting angle of the same specimen for both cases of $\rho = 0.5$ and 2 mm, and once again, the proposed criterion shows more accuracy than PS and MS criteria.

It is worth noting that for a crack problem, which represents a special case of a U-notch when the notch tip radius is zero, the N-ECD-SN criterion should yield identical theoretical predictions to the ECD-SN criterion [55], as both criteria rely on the maximum principal strain component. Therefore, the criterion proposed in the current study offers a more comprehensive version of the previously developed ECD-SN criterion, specifically tailored for V- and U-shaped notches under mixed-mode I/II/III loading conditions.

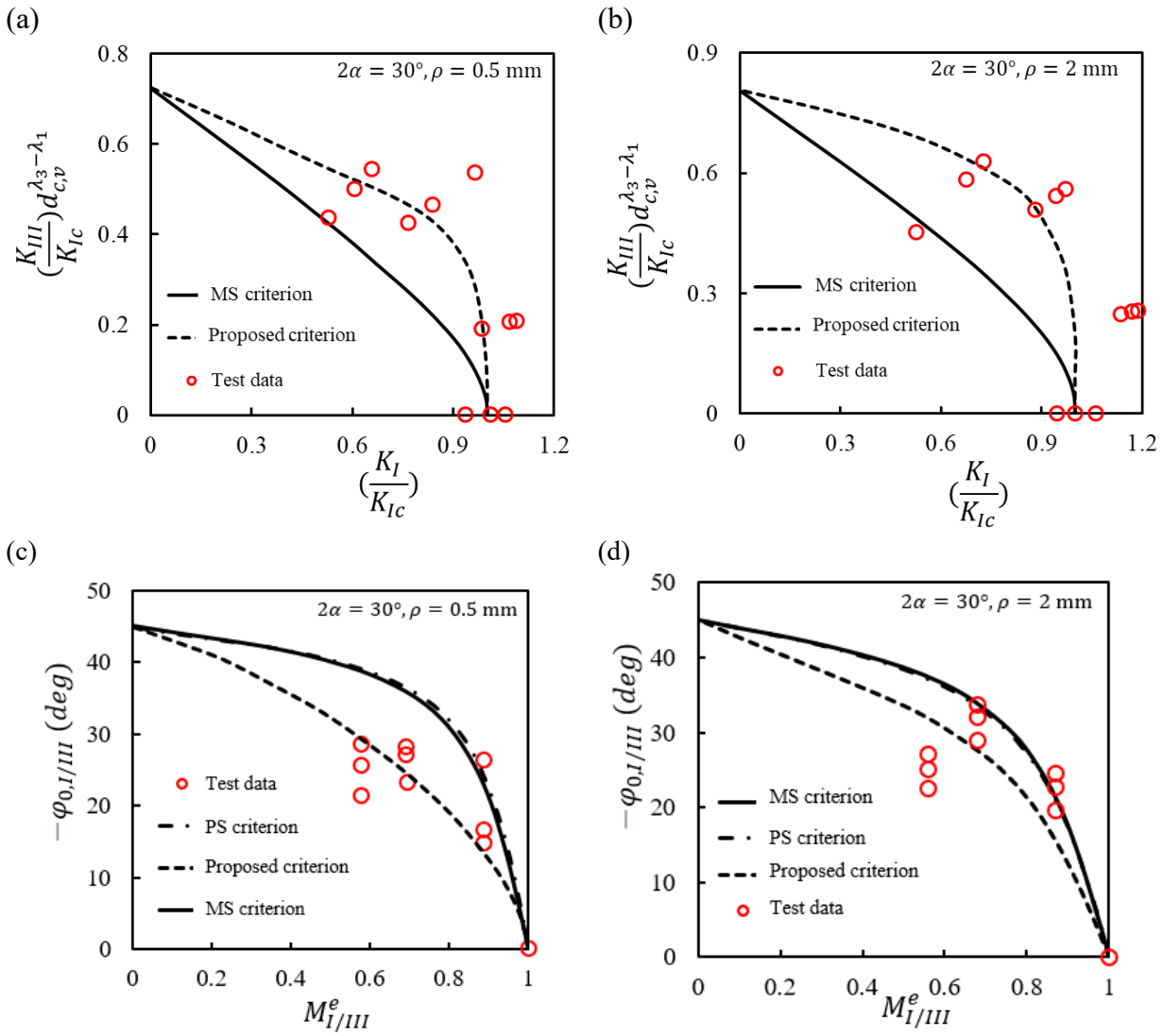

Fig. 8. Theoretical mixed-mode I/III fracture curves by the MS, PS, and N-ECD-SN criteria together with the experimental results for V-notched Polystyrene specimens with the notch opening angle of $2\alpha = 30°$: mixed-mode I/III fracture toughness for a) $\rho = 0.5\ mm$, b) $\rho = 2\ mm$; out-of-plane I/III fracture angle versus different mode mixities for c) $\rho = 0.5mm$, and d) $\rho = 2mm$ [82].

4. Conclusion

By combining the concept of the effective critical distance (ECD) and the maximum principal strain (MPSN) criterion, the new criterion of N-ECD-SN is developed which is suitable for predicting the three-dimensional fracture behavior in components weakened by V- or U-shaped notches. To verify the accuracy of the proposed criterion, the results obtained by the N-ECD-SN

criterion are compared to the theoretical data acquired by means of various well-known fracture criteria together with the experimental data reported in the literature. In this study, U-notched specimens made of graphite and PMMA are considered in which the former is subjected to mixed-mode I/II and the latter is under mixed-mode I/III loading conditions. It is revealed that the N-ECD-SN criterion gives a closer prediction of the test data than the MTS, MS, and PS criteria in all cases. Regarding V-notches, several specimens made of graphite and polystyrene, subjected to mixed-mode I/III loading conditions are studied. This work showed the predicted fracture angles and fracture toughness by the N-ECD-SN criterion are closer to the experimental tests than the ones obtained from MPS and MS criteria. This denotes the superiority of the suggested criterion once again. Moreover, as a good practice and due to the absence of experimental data for specimens weakened by V-notches under II/III loading conditions in the literature, the fracture behavior of such components is theoretically examined by using the N-ECD-SN criterion for different values of p_c, q_c, υ, and the notch opening angle too. According to the current research, the reason behind the higher accuracy of the N-ECD-SN criterion in comparison to its conventional counterparts is that other commonly used criteria such as MTS, MS, MPS, etc. solely consider the length of the processing zone under pure mode I loading conditions and neglect its variation when the loading mode changes. However, the N-ECD-SN criterion refrains from doing so and includes the change in the length of the damage zone corresponding to each mode in the solution which is more realistic and closer to the physics of the problem. Finally, it is worth mentioning that while the proposed criterion has been validated using experimental data for graphite, polymethyl methacrylate, and polystyrene, it can also be applied to a wide range of isotropic materials such as rocks. Additionally, it can be further improved for anisotropic materials like anisotropic rocks.

However, further mixed-mode I/II/III experiments on notched components are necessary for broader validation in the future.

Declaration of interest

None.

Acknowledgements

The authors would like to acknowledge National Science Foundation of the United States (NSF), CMMI program, Mechanics of Materials and Structures (award # 2317406) for the financial support of this research.

Appendix A

(a) V-notch stress field angular functions for mode *I* and *II* [76, 77]:

$$\begin{Bmatrix} X_{\theta\theta} \\ X_{rr} \\ X_{r\theta} \end{Bmatrix}^{I} = \frac{1}{1+\lambda_1+\chi_{b_1}(1-\lambda_1)} \left[\begin{Bmatrix} (1+\lambda_1)\cos(1-\lambda_1)\theta \\ (3-\lambda_1)\cos(1-\lambda_1)\theta \\ (1-\lambda_1)\sin(1-\lambda_1)\theta \end{Bmatrix} + \chi_{b_1}(1-\lambda_1) \begin{Bmatrix} \cos(1+\lambda_1)\theta \\ -\cos(1+\lambda_1)\theta \\ \sin(1+\lambda_1)\theta \end{Bmatrix} \right],$$

$$\begin{Bmatrix} Y_{\theta\theta} \\ Y_{rr} \\ Y_{r\theta} \end{Bmatrix}^{I} = \frac{q}{4(q-1)[1+\lambda_1+\chi_{b_1}(1-\lambda_1)]} \left[\chi_{d_1} \begin{Bmatrix} (1+\mu_1)\cos(1-\mu_1)\theta \\ (3-\mu_1)\cos(1-\mu_1)\theta \\ (1-\mu_1)\sin(1-\mu_1)\theta \end{Bmatrix} + \chi_{c_1} \begin{Bmatrix} \cos(1+\mu_1)\theta \\ -\cos(1+\mu_1)\theta \\ \sin(1+\mu_1)\theta \end{Bmatrix} \right],$$

$$\begin{Bmatrix} X_{\theta\theta} \\ X_{rr} \\ X_{r\theta} \end{Bmatrix}^{II} = \frac{1}{1-\lambda_2+\chi_{b_2}(1+\lambda_2)} \left[\begin{Bmatrix} (1+\lambda_2)\sin(1-\lambda_2)\theta \\ (3-\lambda_2)\sin(1-\lambda_2)\theta \\ (1-\lambda_2)\cos(1-\lambda_2)\theta \end{Bmatrix} + \chi_{b_2}(1+\lambda_2) \begin{Bmatrix} \sin(1+\lambda_2)\theta \\ -\sin(1+\lambda_2)\theta \\ \cos(1+\lambda_2)\theta \end{Bmatrix} \right],$$

$$\begin{Bmatrix} Y_{\theta\theta} \\ Y_{rr} \\ Y_{r\theta} \end{Bmatrix}^{II} = \frac{1}{4(\mu_2-1)[1-\lambda_2+\chi_{b_2}(1+\lambda_2)]} \left[\chi_{d_2} \begin{Bmatrix} (1+\mu_2)\sin(1-\mu_2)\theta \\ (3-\mu_2)\sin(1-\mu_2)\theta \\ (1-\mu_2)\cos(1-\mu_2)\theta \end{Bmatrix} + \chi_{c_2} \begin{Bmatrix} -\sin(1+\mu_2)\theta \\ \sin(1+\mu_2)\theta \\ -\cos(1+\mu_2)\theta \end{Bmatrix} \right],$$

(b) Table A1: Mode *I* eigenvalues for various notch opening angles (2α) [76, 77]:

2α (deg.)	λ_1	μ_1	χ_{b_1}	χ_{c_1}	χ_{d_1}
0	0.5	-0.5	1	4	0
$\pi/6$	0.5014	-0.456	1.0707	3.7907	0.0632
$\pi/4$	0.5050	-0.4319	1.1656	3.572	0.0828
$\pi/3$	0.5122	-0.4057	1.3123	3.2832	0.0960
$\pi/2$	0.5448	-0.3449	1.8414	2.5057	0.1046

$2\pi/3$	0.6157	-0.2678	3.0027	1.5150	0.0871
$3\pi/4$	0.6736	-0.2198	4.1530	0.9933	0.0673
$5\pi/6$	0.7520	-0.1624	6.3617	0.5137	0.0413

(c) Table A2: Mode *II* eigenvalues for various notch opening angles (2α) [77, 67]:

2α (deg.)	λ_2	μ_2	χ_{b_2}	χ_{c_2}	χ_{d_2}
0	0.5	-0.5	1	-12	0
$\pi/6$	0.5982	-0.4465	0.9212	11.3503	-0.3506
$\pi/4$	0.6597	-0.4118	0.8140	10.1876	-0.4510
$\pi/3$	0.7309	-0.3731	0.6584	-8.3946	-0.4788
$\pi/2$	0.9085	-0.2882	0.2189	-2.9382	-0.2436
$2\pi/3$	1.1489	-0.1980	-0.3139	4.5604	0.5133
$3\pi/4$	1.3021	-0.1514	-0.5695	8.7371	1.1362
$5\pi/6$	1.4858	-0.1034	-0.7869	12.9161	1.9376

References

[1] Majidi HR, Razavi SM, Torabi AR. Application of EMC-J criterion to fracture prediction of U-notched polymeric specimens with nonlinear behaviour. Fatigue Fract Eng Mater Struct 2019 Jan;42(1):352-62.

[2] Torabi AR, Shahbazian B. Semi-analytical estimation of the effective plastic zone size at U-notch neighborhood in thin sheets under mixed mode I/II loading. Eng Fract Mech 2020 Nov 1;239:107323.

[3] Saboori B, Ayatollahi MR, Torabi AR, Berto F. Mixed mode I/III brittle fracture in round-tip V-notches. Theor Appl Fract Mech 2016 Jun 1;83:135-51.

[4] Shi SQ, Puls MP. A simple method of estimating the maximum normal stress and plastic zone size at a shallow notch. Int J Pres Ves Pip 64 (1995) 67–71.

[5] Caputo F, Lamanna G, Soprano A. An analytical formulation for the plastic deformation at the tip of short cracks. Procedia Eng 10 (2011) 2988–2993.

[6] Fan M, Yi DK, Xiao ZM. Generalized Irwin plastic zone correction for a Griffith crack near a coated-circular inclusion. Int. J. Damage Mech. 24 (2014) 663–682.

[7] Torabi AR, Shahbazian B, Mirsayar M, Cicero S. A Methodology to Determine the Effective Plastic Zone Size Around Blunt V-Notches under Mixed Mode I/II Loading and Plane-Stress Conditions. Metals 2021 Jun 29;11(7):1042.

[8] Zhou XP, Shou YD, Berto F. Analysis of the plastic zone near the crack tips under the uniaxial tension using ordinary state-based peridynamics. Fatigue Fract Eng Mater Struct 41 (2017) 1159–1170.

[9] Torabi AR, Shahbazian B. Notch tip plastic zone determination by extending Irwin's model. Theor Appl Fract Mech 2020 Aug 1;108:102643.

[10] Pratap CR, Pandey RK. Effect of geometry and finite root radius on plastic zone and tip opening displacement, Eng Fract Mech 19 (1984) 849–861.

[11] Yi H, Jingjie C, Gang L. A new method of plastic zone size determined based on maximum crack opening displacement. Eng Fract Mech 2010;77:2912–8.

[12] Kang KJ, Beom HG. Plastic zone size near the crack tip in a constrained ductile layer under mixed mode loading. Eng Fract Mech 2000;66(3):257–68.

[13] Hussain MA, Pu SL, Underwood J. Strain energy release rate for a crack under combined mode I and mode II. In Fracture analysis: Proceedings of the 1973 national symposium on fracture mechanics, part II 1974 Jan. ASTM International.

[14] Sih GC. Strain-energy-density factor applied to mixed mode crack problems. Int J fract 1974;10(3):305-21.

[15] Berto F, Lazzarin P, Livieri P. On the second non-singular stress term of the V-notch solution: a new engineering solution. Int J fract 2013 May;181(1):83-98.

[16] Zhao Y. Griffith's criterion for mixed mode crack propagation. Eng Fract Mech 1987;26(5):683-9.

[17] Chang J, Xu JQ, Mutoh Y. A general mixed-mode brittle fracture criterion for cracked materials. Eng Fract Mech 2006;73(9):1249-63.

[18] Bidadi, J., Aliha, M. R. M., & Akbardoost, J. Development of maximum tangential strain (MTSN) criterion for prediction of mixed-mode I/III brittle fracture. *International* Journal of Solids and Structures, 2022; 256, 111979.

[19] Sih GC, Cha BC. A fracture criterion for three-dimensional crack problems. Eng Fract Mech 1974;6(4):699-723.

[20] Sih GC. A review of the three-dimensional stress problem for a cracked plate. Int J Fract Mech 1971;7(1):39-61.

[21] Wang Q, Feng YT, Zhou W, Cheng Y, Ma G. A phase-field model for mixed-mode fracture based on a unified tensile fracture criterion. Comput Methods Appl Mech Eng 2020; 370:113270.

[22] Mirsayar MM. Mixed mode fracture analysis using extended maximum tangential strain criterion. Mater Des 2015; 86:941-7.

[23] Chang KJ. On the maximum strain criterion—a new approach to the angled crack problem. Eng Fract Mech 1981;14(1):107-24.

[24] Mirsayar MM, Berto F, Aliha MR, Park P. Strain-based criteria for mixed-mode fracture of polycrystalline graphite. Eng Fract Mech 2016; 156:114-23.

[25] Mirsayar MM. T-strain effects in kinked interfacial fracture of bonded composites. Theor Appl Fract Mech 2019; 104:102381.

[26] Mirsayar MM. On the low temperature mixed mode fracture analysis of asphalt binder–Theories and experiments. Eng Fract Mech 2017; 186:181-94.

[27] Mirsayar MM. On fracture analysis of dental restorative materials under combined tensile-shear loading. Theor Appl Fract Mech 2018; 93:170-6.

[28] Mirsayar MM, Park P. Mixed mode brittle fracture analysis of high strength cement mortar using strain-based criteria. Theor Appl Fract Mech 2016; 86:233-8.

[29] Mirsayar MM, Razmi A, Aliha MR, Berto F. EMTSN criterion for evaluating mixed mode I/II crack propagation in rock materials. Eng Fract Mech 2018; 190:186-97.

[30] Erdogan F, Sih GC. On the crack extension in plates under plane loading and transverse shear. J Basic Eng 1963; 85, 519–527.

[31] Shen, Z., Yu, H., Guo, L., Hao, L., Zhu, S., & Huang, K. (2023). A modified 3D G-criterion for the prediction of crack propagation under mixed mode I-III loadings. Engineering Fracture Mechanics, 281, 109082.

[32] Liu S, Chao YJ, Zhu X. Tensile-shear transition in mixed mode I/III fracture. Int J Solids Struct 2004;41(22-23):6147-72.

[33] Sajjadi SH, Salimi-Majd D, Ghorabi MO. Development of a brittle fracture criterion for prediction of crack propagation path under general mixed mode loading. Eng Fract Mech 2016;155:36-48.

[34] Tai YH, Brown MW, Yates JR. A new solution for 3D crack extension based on linear elastic stress fields. Eng Fract Mech 2011;78(8):1602-13.

[35] Smith DJ, Ayatollahi MR, Pavier MJ. The role of T-stress in brittle fracture for linear elastic materials under mixed-mode loading. Fatigue Fract Eng Mater Struct 2001;24(2):137-50.

[36] Wang X, Lewis T, Bell R. Estimations of the T-stress for small cracks at notches. Eng Fract Mech 2006 Feb 1;73(3):366-75.

[37] Meliani MH, Azari Z, Pluvinage G, Matvienko YG. The effective T-stress estimation and crack paths emanating from U-notches. Eng Fract Mech 2010 Jul 1;77(11):1682-92.

[38] Ayatollahi MR, Dehghany M. On T-stresses near V-notches. Int J Fract 2010 Sep;165(1):121-6.

[39] Mirsayar MM. On fracture of kinked interface cracks–The role of T-stress. Mater Des 2014; 61:117-23.

[40] Ayatollahi MR, Saboori B. T-stress effects in mixed mode I/II/III brittle fracture. Eng Fract Mech 2015; 144:32-45.

[41] Erdogan F, Sih GC. On the crack extension in plates under plane loading and transverse shear. J Basic Eng 1963;85:519–27.

[42] Schöllmann M, Richard HA, Kullmer G, Fulland M. A new criterion for the prediction of crack development in multiaxially loaded structures. Int J Fract 2002; 117(2):129–41.

[43] Liu S, Chao YJ, Zhu X. Tensile-shear transition in mixed mode I/III fracture. Int J Solids Struct 2004;41(22–23):6147–72.

[44] Ayatollahi MR, Torabi AR. Brittle fracture in rounded-tip Vshaped notches. Mater Des 2010;31:60–7.

[45] Razavi SM, Berto F. A new fixture for fracture tests under mixed mode I/II/III loading. Fatigue Fract Eng Mater Struct 2019;42(9):1874–88.

[46] Ayatollahi MR, Saboori B. A new fixture for fracture tests under mixed mode I/III loading. European J Mech-A/Solids 2015;51:67–76.

[47] Zeinedini A. A novel fixture for mixed mode I/II/III fracture testing of brittle materials. Fatigue Fract Engng Mater Struct 2019;42(4):838–53.

[48] Ayhan AO, Demir O. A novel test system for mixed mode-I/II/III fracture tests–Part 1: Modeling and numerical analyses. Eng Fract Mech 2019;218:106597.

[49] Deng X, Sutton MA, Zuo J, Wang L. Mixed-mode fracture analysis of airframe materials. In: Proceedings of the fifth Joint NASA/FAA/DoD conference on aging aircraft, Kissimmee, FL September 2001;10–13.

[50] Pook LP. Comments on fatigue crack growth under mixed modes I and III and pure mode III loading. Multiaxial Fatigue, ASTM STP 853. Philadelphia: American Society for Testing and Materials 1985;249–263.

[51] Richard, H. A., Schramm, B., & Schirmeisen, N. H. Cracks on mixed mode loading–theories, experiments, simulations. International Journal of Fatigue, 2014; 62, 93-103.

[52] Ayatollahi MR, Saboori B. Maximum tangential strain energy density criterion for general mixed mode I/II/III brittle fracture. Int J Damage Mech 2015;24(2): 263–78.

[53] Mirsayar MM. A generalized criterion for fatigue crack growth in additively manufactured materials–build orientation and geometry effects. Int J Fatigue 2021; 145:106099.

[54] Mirsayar MM. Maximum principal strain criterion for fracture in orthotropic composites under combined tensile/shear loading. Theor Appl Fract Mech 2022; 118:103291.

[55] Mirsayar MM. On the effective critical distances in three-dimensional brittle fracture via a strain-based framework. Eng Fract Mech 2021; 248:107740.

[56] Li, S., Lu, H., Huang, X., Qin, R., & Mao, J. Sensitivity analysis of notch shape on brittle failure by using uni-bond dual-parameter peridynamics. *Engineering Fracture Mechanics*, 2023; *291*, 109566.

[57] Yang, D., He, X., & Deng, Y. An effective correspondence-based peridynamics-FEM coupling model for brittle fracture. *International Journal of Mechanical Sciences*, 2024; *264*, 108815.

[58] Mirsayar, M. A generalized model for dynamic mixed-mode fracture via state-based peridynamics. *Fatigue & Fracture of Engineering Materials & Structures*, 2023; *46*(1), 244-258.

[59] Liu, R., Xue, Y., & Li, S. (2023). A three-dimensional (3D) micro-potential-based peridynamics model for deformation and fracture in solid materials. *Engineering Fracture Mechanics*, *282*, 109180.

[60] Kumar, A., Ravi-Chandar, K., & Lopez-Pamies, O. The revisited phase-field approach to brittle fracture: application to indentation and notch problems. *International Journal of Fracture*, 2022; *237*(1-2), 83-100.

[61] Yue, Q., Wang, Q., Zhou, W., Rabczuk, T., Zhuang, X., Liu, B., & Chang, X. (2023). An efficient adaptive length scale insensitive phase-field model for three-dimensional fracture of solids using trilinear multi-node elements. *International Journal of Mechanical Sciences*, *253*, 108351.

[62] Li, C., Fang, J., Wan, Y., Qiu, N., Steven, G., & Li, Q. (2023). Phase field fracture model for additively manufactured metallic materials. *International Journal of Mechanical Sciences*, *251*, 108324.

[63] Wu, J. Y., Huang, Y., Zhou, H., & Nguyen, V. P. Three-dimensional phase-field modeling of mode I+ II/III failure in solids. *Computer Methods in Applied Mechanics and Engineering*, 2021; *373*, 113537.

[64] Mukhtar, F. M., Alves, P. D., & Duarte, C. A. (2020). Validation of a 3-D adaptive stable generalized/eXtended finite element method for mixed-mode brittle fracture propagation. *International Journal of Fracture*, *225*(2), 129-152.

[65] Shi, F., Wang, D., & Yang, Q. An XFEM-based numerical strategy to model three-dimensional fracture propagation regarding crack front segmentation. *Theoretical and Applied Fracture Mechanics*, 2022; *118*, 103250.

[66] Taylor D. The theory of critical distances. Eng Fract Mech 2008;75(7):1696-705.

[67] Susmel L, Taylor D. The theory of critical distances to predict static strength of notched brittle components subjected to mixed-mode loading. Eng Fract Mech 2008 Feb 1;75(3-4):534-50.

[68] Susmel L. The theory of critical distances: a review of its applications in fatigue. Eng Fract Mech 2008;75(7):1706-24.

[69] Mirsayar MM, Shahbazian B. An energy-based criterion for mixed-mode I/II/III fracture considering effective critical distances. Eng Fract Mech 2022 Sep 1;272:108674.

[70] Shahbazian B, Mirsayar MM, Aliha MR, Darvish MG, Asadi MM, Haghighatpour PJ. Experimental and theoretical investigation of mixed-mode I/II and I/III fracture behavior of PUR foams using a novel strain-based criterion. Int J Solids Struct 2022 Dec 15;258:111996.

[71] Riazi, R., Torabi, A. R., Amininejad, S. H., & Sabour, M. H. Combined tension–shear fracture analysis of V-notches with end holes. Acta Mechanica, 2015; 226, 3717-3736.

[72] Seweryn A. Brittle fracture criterion for structures with sharp notches. Eng Fract Mech 47 (1994) 673–681.

[73] Ayatollahi MR, Torabi AR. Brittle fracture in rounded-tip V-shaped notches. Mater Des 31 (2010) 60–67.

[74] M.R. Ayatollahi, A.R. Torabi. Tensile fracture in notched polycrystalline graphite specimens. Carbon 48 (2010) 2255–2265.

[75] Williams ML. Stress singularities resulting from various boundary conditions in

angular corners of plates in extension. J Appl Mech 19 (1952) 526–528.

[76] Filippi S, Lazzarin P, Tovo R. Developments of some explicit formulas useful to describe elastic stress fields ahead of notches in plates. Int J Solids Struct 2002 Aug 1;39(17):4543-65.

[77] Zappalorto M, Lazzarin P, Filippi S. Stress field equations for U and blunt V-shaped notches in axisymmetric shafts under torsion. Int J Fract 2010 Aug;164:253-69.

[78] Berto F, Campagnolo A, Ayatollahi MR. Brittle fracture of rounded V-notches in isostatic graphite under static multiaxial loading. Phys Mesomech 2015 Oct;18:283-97.

[79] Torabi AR, Fakoor M, Pirhadi E. Fracture analysis of U-notched disc-type graphite specimens under mixed mode loading. Int J Solids Struct 2014 Mar 15;51(6):1287-98.

[80] Saboori B, Torabi AR, Ayatollahi MR, Berto F. Experimental verification of two stress-based criteria for mixed mode I/III brittle fracture assessment of U-notched components. Eng Fract Mech 2017 Sep 1;182:229-44.

[81] Saboori B, Ayatollahi MR, Torabi AR, Berto F. Mixed mode I/III brittle fracture in round-tip V-notches. Theor Appl Fract Mech 2016 Jun 1;83:135-51.

[82] Saboori B, Torabi AR, Mohammadian SK. Experimental and stress-based theoretical studies on mixed mode I/III fracture of round-tip V-notched Polystyrene specimens. Theor Appl Fract Mech 2018 Jun 1;95:283-305.